nature geoscience

LETTERS

PUBLISHED ONLINE: 26 JULY 2009 | DOI: 10.1038/NGEO590

Tectonic evolution of the Salton Sea inferred from seismic reflection data

D. S. Brothers[1]*, N. W. Driscoll[1], G. M. Kent[1], A. J. Harding[1], J. M. Babcock[1] and R. L. Baskin[2]

Oblique extension across strike-slip faults causes subsidence and leads to the formation of pull-apart basins such as the Salton Sea in southern California. The formation of these basins has generally been studied using laboratory experiments or numerical models[1–4]. Here we combine seismic reflection data and geological observations from the Salton Sea to understand the evolution of this nascent pull-apart basin. Our data reveal the presence of a northeast-trending hinge zone that separates the sea into northern and southern sub-basins. Differential subsidence (>10 mm yr^{-1}) in the southern sub-basin suggests the existence of northwest-dipping basin-bounding faults near the southern shoreline, which may control the spatial distribution of young volcanism. Rotated and truncated strata north of the hinge zone suggest that the onset of extension associated with this pull-apart basin began after ~0.5 million years ago. We suggest that slip is partitioned spatially and temporally into vertical and horizontal domains in the Salton Sea. In contrast to previous models based on historical seismicity patterns[5], the rapid subsidence and fault architecture that we document in the southern part of the sea are consistent with experimental models for pull-apart basins[1].

Our current understanding of the kinematics and evolution of pull-apart basins is based largely on laboratory[1–3] and numerical models[4], with few well-dated field studies examining the regional deformation patterns within active pull-apart basins. The San Andreas fault–Imperial fault (SAF–IF) transtensional step-over is an ideal locale to study the relationship between horizontal and vertical deformation in an active pull-apart basin using regional-scale, high-resolution geophysical methods[6]. This step-over delineates the northward transition from the obliquely divergent Gulf of California margin to transpressional deformation of the San Andreas fault system. Early crustal models suggested that much of the southern Salton Trough is underlain and intruded by young, mafic material[7,8]. Geophysical and thermal anomalies along with volcanism near the southern Salton Sea were attributed to a buried spreading centre between the SAF and IF (refs 7, 8). Later studies examined seismicity patterns and the kinematics of moderate-to-strong earthquakes in the region[9–11]. The complex ladder-like seismicity patterns of the Brawley Seismic Zone (BSZ; Fig. 1) and faulting to the west of the Salton Sea led to models of distributed dextral shear and block rotation between the SAF and San Jacinto fault (SJF; ref. 5). At present, a consistent model for basin evolution is needed that accounts for the high subsidence rates observed in this study, the seismicity patterns[11], the prominent northeast-trending thermal anomaly[12] and string of Quaternary volcanic buttes[13] (Fig. 1).

Between 2006 and 2008, we acquired over 1,000 line-km of high-resolution chirp seismic reflection data in the Salton Sea (Fig. 1). Sediments deposited during the late Holocene in Lake Cahuilla[14] (herein referenced as the Cahuilla Formation, CFm) blanket the basin and are defined by parasequence sets that have been radiocarbon dated at onshore sites[15]. The sedimentary packages record shoreline fluctuations of Lake Cahuilla, enabling us to correlate high- and low-amplitude reflectors offshore with dated sequences onshore. In the Salton Sea, the CFm records deformation for at least 12 transgression–regression cycles (~2–3 kyr BP). Numerous faults are identified in the CFm by vertically offset reflectors and occasionally by seafloor scarps. Potential correlations between onshore and offshore structures include the Extra fault zone[9,16] (EFZ) and possibly the Elmore Ranch fault[17] (ERF); both show sinistral slip west of the Salton Sea. Although historic seismicity is scarce along the newly mapped faults[5,11], palaeoearthquakes have produced over 1 m of vertical offset per event (see Supplementary Fig. S4). The average strike of faults in the southern sea (N15° E; Fig. 1c) is more northerly than the cross-faults west of the Salton Sea and the short (<5 km) ~N40° E trending seismicity lineaments in the BSZ.

The northeast-striking EFZ, expressed in the CFm as a series of down-to-the-southeast growth folds and faults, seems to be a structural hinge zone that separates the sea into northern and southern basins (Fig. 2). In the northern basin, an angular unconformity separates parallel, concordant reflectors of the CFm from underlying folded and faulted reflectors that we interpret as the Pleistocene Brawley Formation[16,18] (BFm) mapped west of the sea and at Durmid Hill (DH) (Fig. 1). BFm strata show a progressive increase in dip and fold frequency southward approaching the EFZ, then drop below the limits of acoustic penetration south of the EFZ. The fold geometry provides evidence for broad ~N/S-directed compression and uplift that was subsequently truncated, leaving a nearly flat unconformity surface. The trend of the compression seems to align with subtle topography associated with the San Felipe Anticline west of the sea[16] (Fig. 1). Nevertheless, we do not observe stratigraphic evidence within the CFm for differential subsidence or uplift north of the EFZ.

The EFZ marks the northern limit of active extension. South of the EFZ, CFm beds show marked divergence and evidence for syntectonic sedimentation. Average subsidence measured over the AD 830 time-horizon just south of the hinge zone is between 9 and 12 mm yr^{-1} (Fig. 2; Supplementary Fig. S3). The CFm beds continue to diverge to the southeast beyond our data coverage, suggesting that the above estimate is a minimum. Stratal divergence indicates that subsidence is equal to or slightly higher than sedimentation, where the average sedimentation rate in the southern basin has been nearly 19 mm yr^{-1} since ~AD 1360. The projected location of maximum subsidence is near the southern shoreline, approximately coincident with the locus of Quaternary volcanism and a northeast-trending band of very high heat flow. Farther south, the rapidly subsiding Mesquite Basin bounds the

[1]Scripps Institution of Oceanography, University of California, San Diego, 9500, Gilman Drive, La Jolla, California 92093, USA, [2]United States Geological Survey, 2329 West Orton Circle, West Valley City, Utah 84119, USA. *e-mail: dbrother@ucsd.edu.

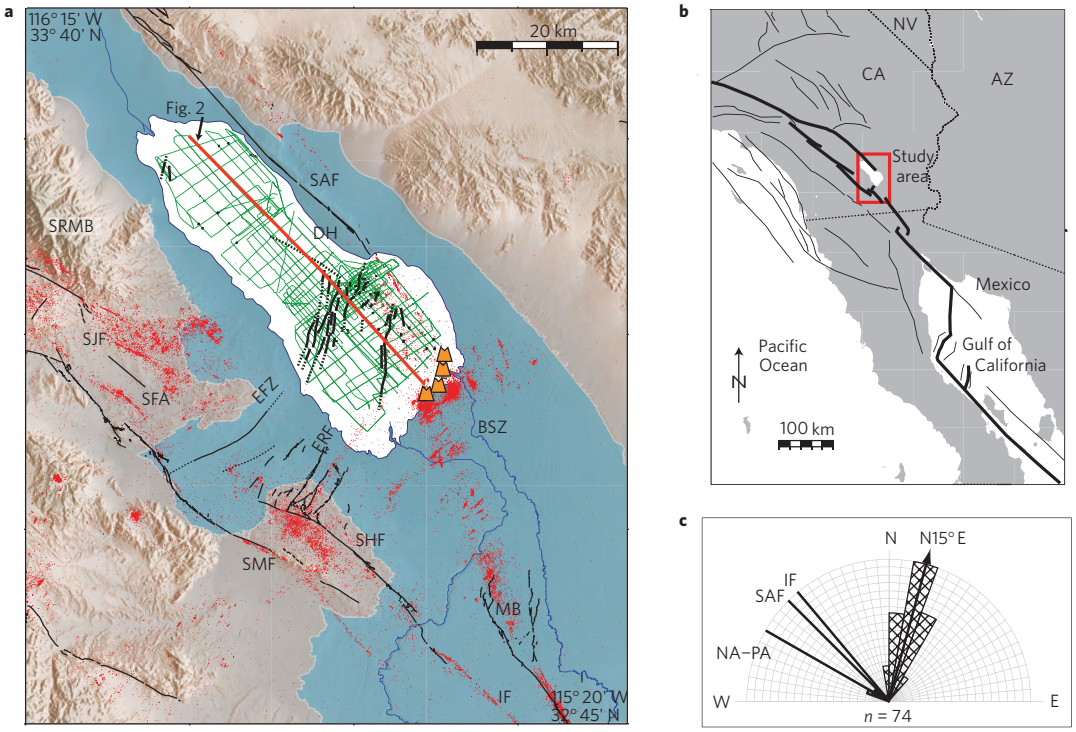

Figure 1 | Map of the Salton Sea region. a, Green lines represent seismic reflection profiles (the red line is the location for Fig. 2). Lake Cahuilla is shaded blue. Black lines denote Holocene faults, red dots are relocated earthquakes[11] and orange triangles are volcanic buttes. Abbreviations: SRMB, Santa Rosa mountain block; SJF, San Jacinto fault; EFZ, Extra fault zone; ERF, Elmore Ranch fault; BSZ, Brawley seismic zone; SAF, San Andreas fault; SHF, Superstition Hills fault; SMF, Superstition Mountain fault; IF, Imperial fault; DH, Durmid Hill; SFA, San Felipe anticline; MB, Mesquite basin. **b**, Regional map of study area. Abbreviations: CA, California; AZ, Arizona; NV, Nevada. **c**, Rose diagram of fault strikes. The average strike for faults in the sea is N15° E (see the Methods section). Other trends are the SAF, IF and North America–Pacific (NA–PA) plate motion vector at this latitude[30].

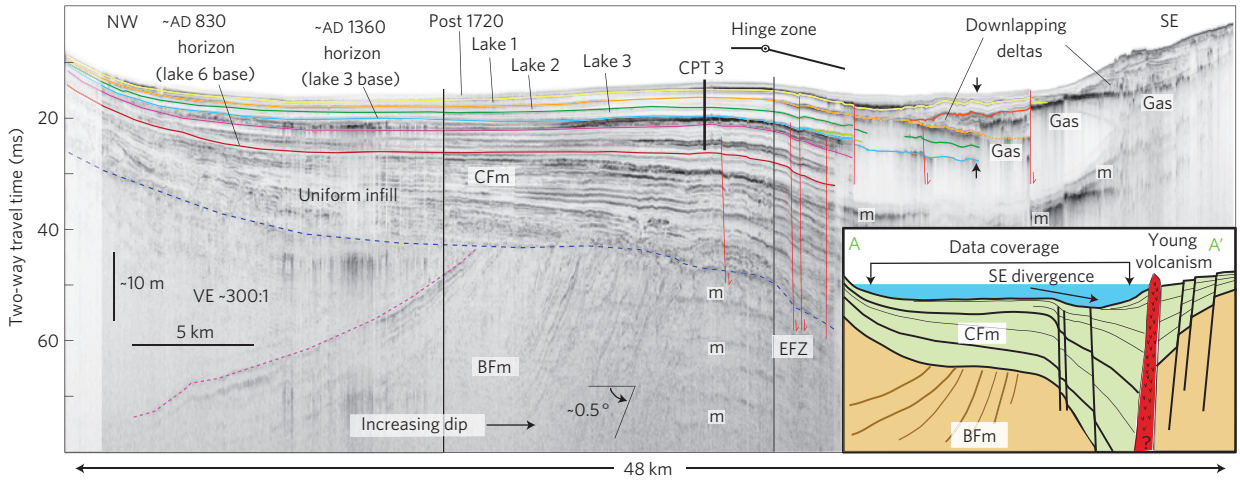

Figure 2 | Salton Sea long-axis seismic reflection profile. A truncation surface (dashed blue line) separates the Holocene CFm from the underlying Pleistocene BFm. Coloured horizons represent time horizons in the CFm; red lines denote faults; black arrows mark the location at which sedimentation rate was estimated; multiple reflections (acoustic artefacts) are identified by 'm'. The black pipe labelled CPT-3 represents cone penetration test data (see Supplementary Fig. S1). Inset, Interpretive cross-section. North of the EFZ, reflectors in the CFm are concordant and record little deformation. Reflectors in the BFm show evidence for ~N/S-oriented compression. South of the EFZ, layers diverge and thicken. We infer that maximum subsidence occurs near the southern shoreline and that extensional faults may provide fluid migration pathways for young volcanism.

northern terminus of the IF and seems to define a separate pull-apart basin[19,20] within the larger SAF–IF step-over (Fig. 1).

If we assume that subsidence is equal to or slightly greater than sedimentation (~20 mm yr^{-1}) and that an inferred boundary fault (assumed strike/dip = N30° E/60° N) accommodates most of the subsidence, then horizontal extension is calculated at 11.5 mm yr^{-1} in the direction N60° W (orthogonal to the boundary fault). Projected onto an azimuth parallel to the SAF, this yields ~11.2 mm yr^{-1} of dextral slip. Although long-term slip-rate estimates for the southern SAF are few and somewhat controversial, offset alluvial fans north of the Salton Sea provide a rate between 9 and 15 mm yr^{-1} over the past 45–50 kyr (ref. 21), whereas the short-term geodetic rate is 23.3 ± 0.5 mm yr^{-1} (ref. 22). Should the long-term rate be more representative, 75–100% of the horizontal

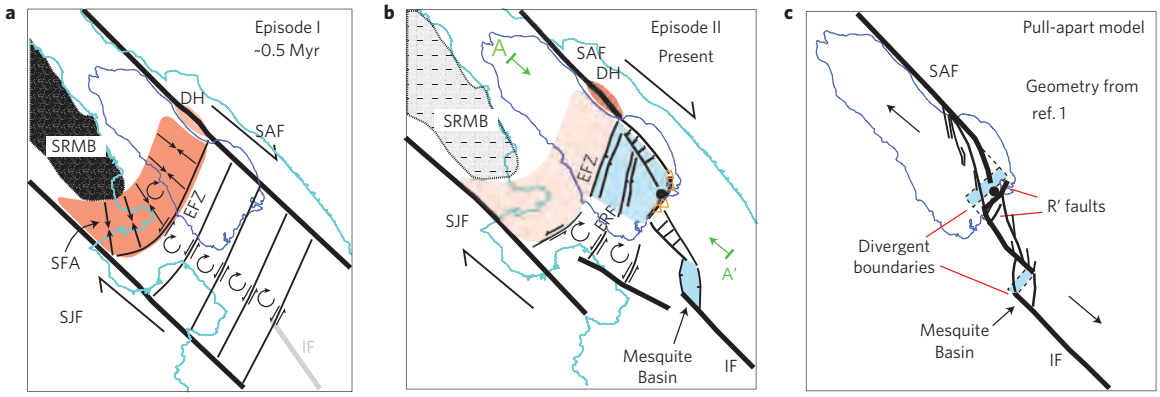

Figure 3 | Map-view models for the tectonic evolution of the Salton Sea. Bold faults represent the primary tectonic structures; orange triangles are volcanic buttes[13]. Blue shades are extensional domains; light-red zones are inactive compression; dark-red zones are active compression; the blue line is the Lake Cahuilla high-shoreline. Green arrows define the extent of the cross-sectional view in Fig. 2 (inset). **a**, Block rotation between the SAF and the SJF and compression north of the EFZ at ~0.5 Myr. **b**, Development of SAF–IF step-over and present-day configuration. **c**, Physical model of a pull-apart basin with mechanical layering[1] (superimposed on the Salton Sea). Extension is focused along R′ faults above the divergent boundary, forming an asymmetric basin. The Mesquite Basin represents a separate pull-apart basin within the SAF–IF step-over.

slip transferred from the SAF into the Salton Sea is accommodated by extension and subsidence, leaving less than 4 mm yr^{-1} for intrabasin strike-slip faulting and/or rotation. If we assume that the geodetic rate is more representative, then only ~50% of SAF slip is converted to extension in the sea. The ratio of horizontal slip to vertical subsidence constrains the relative importance of slip partitioning in this evolving pull-apart basin.

The EFZ and projected ERF show consistent down-to-the-east vertical displacement beneath the Salton Sea; these observations call into question the relationship between the onshore and offshore structures. If they represent the same fault segments, their trends and kinematics change as they extend into the SAF–IF step-over. Studies examining cross-faults west of the Salton Sea and seismicity in the BSZ (refs 5, 9, 23) would not have observed the large component of extension and subsidence occurring within the sea. We contend that the ~N15° E striking faults and inferred boundary fault in the southern sea produce relatively infrequent, but large, earthquakes (magnitude $M > 6$) that accommodate extension and subsidence, whereas the smaller events ($M < 5$) and microseismicity that define the BSZ are due to fracturing and block rotation within a narrow (<5-km-wide), dextral shear zone. In essence, the southern sea seems to be slip-partitioned into two separate tectonic domains. Contrary to previous models[5], we argue that block rotation alone cannot generate the observed rapid subsidence, the northeast-trending collection of volcanic buttes, and the thermal and geophysical anomalies along the southern shoreline[8,12,13]. These observations are more consistent with a large component of extension. Understanding the kinematics of the SAF–IF step-over may depend on the observation timescale. Extension and subsidence dominate over hundreds of years through ground-rupturing ($M > 6$) normal-oblique earthquakes, where the BSZ releases strain over decadal scales through numerous small-to-moderate earthquakes[10,11] and aseismic processes[24]. Sinistral cross-faults west of the Salton Sea have low slip-rates (~1 mm yr^{-1}; ref. 23) and seem to be secondary structures responding to rotation within the broader SAF–SJF strain field[5].

We propose a conceptual two-stage model for tectonic evolution for the Salton Sea. Though poorly understood, Episode I is characterized by the transpression observed north of the EFZ. Here, the EFZ may have started as a transpressional boundary between the SAF and SJF, before the development of the SAF–IF step-over (Fig. 3a). As the SJF formed, clockwise rotating blocks bounded by northeast-striking sinistral faults accommodated strain distributed between the SAF and SJF (ref. 5). One scenario is that block boundaries were not defined by simple, linear faults, but contained geometric complexities that produced vertical deformation. As rotation proceeded, block margins west of the Salton Sea are expected to have translated northward, impinging onto the Santa Rosa Mountains and resulting in ~N/S-oriented compression recorded in the sediments beneath the Salton Sea.

Episode II marks the onset of extension in the Salton Sea and development of the present-day transtensional regime (Fig. 3b). As the SAF–IF step-over formed, compression waned and some of the cross-faults that formed during Episode I began to accommodate normal slip. The differential subsidence and normal slip observed across northeast-striking faults began with the formation or northward propagation of the IF. Fault and subsidence patterns support bulk surface displacement being roughly parallel to plate motion. As extension progressed, subsidence became focused in the southern sea along an inferred north-dipping basin-bounding fault zone that we believe resembles R′ faults in physical models of pull-apart basins[1] (Fig. 3b,c). Maximum subsidence occurs in the hanging wall of R′ faults directly above the divergent boundary, producing hinge zone roll-over and stratal divergence[1]. These boundary faults may enhance decompression melting and provide migration pathways for volcanic and hydrothermal fluids (Fig. 2 (inset)). Similarities between observed structure and physical models suggest that the Salton Sea is in an early to mid-stage of development, but the overall SAF–IF step-over is relatively immature[1,2]. Short sinistral faults in the BSZ (ref. 5) may reflect internal deformation and rotation within strike-slip shear zones, as predicted in physical models[1] (Fig. 3b,c). Through time, deformation is expected to broaden where the Salton Sea and Mesquite Basin coalesce to form a composite pull-apart basin[25].

Although the absolute age of each deformational episode remains poorly constrained, this study provides relative ages for the deformation and an upper bound on the age of the SAF–IF step-over. In our model, the compression of the BFm beneath the angular unconformity is contemporaneous with, or postdates, the onset of deformation along the southern SJF zone (1.1–1.3 Myr; ref. 26). Subsequently, a structural reorganization that established N/S-directed compression to the west of the Salton Sea occurred at ~0.5–0.6 Myr (refs 16, 27), approximately the same time that deposition of BFm ended[16]. Assuming that the structural reorganization coincides with Episode I, we argue that the compression in the BFm north of hinge occurred sometime after ~0.5 Myr. Compression was then replaced by extension south of the EFZ, thus providing a maximum age for the formation

of the SAF–IF step-over at ~0.5 Myr. Erosion of onshore BFm strata may present a significant lacuna, therefore a late-Pleistocene[19] (~0.1 Myr) age for the SAF–IF is possible.

In summary, our observations provide important constraints on the growth of an active pull-apart basin and the evolution of the southern SAF system. On the basis of our interpretive model we conclude the following. (1) Differential subsidence south of the EFZ has produced an asymmetric basin with strata thickening southward into a basin-bounding fault system. (2) Transtension beneath the Salton Sea is partitioned into distinct extensional and strike-slip domains. Extensional faults are at a high angle to the SAF, rupture during larger, less frequent earthquakes and should be considered seismically hazardous. The BSZ accommodates dextral shear transferred into the basin through internal deformation (for example secondary faulting and/or rotation). (3) The Salton Sea basin seems similar to young pull-apart basins in physical models and provides a comparative example on the basis of high-fidelity records of deformation. Our proposed model is the first to account for the rapid subsidence, elevated heat flow and profuse seismicity in the Salton Sea.

Methods

Seismic reflection data were collected using Scripps Institution of Oceanography's Edgetech 512i sub-bottom profiler, herein referred to as a chirp system. Each shot was digitally recorded and included real-time GPS navigation. Profiles were processed using SIOSEIS then imported into the Kingdom Suite and IVS Fledermaus software packages for interpretation. Vertical resolution between reflectors is ~15–40 cm, depending on the source pulse and sediment velocity, and vertical penetration is up to ~70 m. Time-to-depth conversions assumed a sediment velocity of 1,600 m s^{-1}. Seismic sections were interpreted using considerable vertical exaggeration (as in Fig. 2) to delineate subtle changes in stratal geometry and identify regional scale variation. All faults shown in Fig. 1 offset the CFm and typically dip between 50° and 70° (faults in Fig. 2 seem vertical owing to vertical exaggeration). Fault statistics (Fig. 1c) were not normalized by fault length because many faults extend beyond the data coverage.

The CFm consists of unconsolidated fluvio-lacustrine facies deposited during Colorado River diversions, but before the formation of the Salton Sea (1905). Between 2003 and 2006, United Research Services collected 17 sediment borings and 34 cone penetration tests in the Salton Sea[28]. These data provide information on the lithostratigraphy that can be correlated with the acoustic properties observed in chirp profiles. High-amplitude horizons correspond to lowered lake levels and the consequent increased silt/sand components detected by cone penetrometer tests[28]; low-amplitude horizons represent fine-grained high-stand lake deposits. Correlating the onshore[15] and offshore lake sequences enables us to establish a chronostratigraphic framework that is used to constrain the deformation history beneath the sea (see Supplementary Fig. S1). The most recent Lake Cahuilla high-stand occurred around AD 1680–1720 and up to six high-stands have been dated back to ~AD 800 (refs 15, 29). Dated horizons were correlated spatially between chirp profiles to construct isopach maps and estimate differential subsidence rates.

Received 6 January 2009; accepted 30 June 2009; published online 26 July 2009

References

1. Basile, C. & Brun, J. P. Transtensional faulting patterns ranging from pull-apart basins to transform continental margins: An experimental investigation. *J. Struct. Geol.* **21**, 23–37 (1999).
2. Wu, J. E., McClay, K., Whitehouse, P. & Dooley, T. 4D analogue modelling of transtensional pull-apart basins. *Mar. Petrol. Geol.* (in the press).
3. McClay, K. & Dooley, T. Analog models of pull-apart basins. *Geology* **23**, 711–714 (1995).
4. Katzman, R., ten Brink, U. S. & Lin, J. A. 3-Dimensional modeling of pull-apart basins—implications for the tectonics of the dead-sea basin. *J. Geophys. Res.* **100**, 6295–6312 (1995).
5. Nicholson, C., Seeber, L., Williams, P. & Sykes, L. R. Seismic evidence for conjugate slip and block rotation within the San-Andreas Fault System, Southern California. *Tectonics* **5**, 629–648 (1986).
6. Seeber, L. *et al.* Rapid subsidence and sedimentation from oblique slip near a bend on the North Anatolian transform fault in the Marmara Sea, Turkey. *Geology* **34**, 933–936 (2006).
7. Elders, W. A., Biehler, S., Rex, R. W., Robinson, P. T. & Meidav, T. Crustal spreading in Southern California. *Science* **178**, 15–24 (1972).
8. Fuis, G. S., Mooney, W. D., Healy, J. H., Mcmechan, G. A. & Lutter, W. J. A seismic refraction survey of the Imperial-Valley Region, California. *J. Geophys. Res.* **89**, 1165–1189 (1984).
9. Hudnut, K. *et al.* Surface ruptures on cross-faults in the 24 November 1987 Superstition Hills, California, earthquake sequence. *Bull. Seismol. Soc. Am.* **79**, 282–296 (1989).
10. Hardebeck, J. L. & Shearer, P. M. Using S/P amplitude ratios to constrain the focal mechanisms of small earthquakes. *Bull. Seismol. Soc. Am.* **93**, 2434–2444 (2003).
11. Lin, G. Q., Shearer, P. M. & Hauksson, E. Applying a three-dimensional velocity model, waveform cross correlation, and cluster analysis to locate southern California seismicity from 1981 to 2005. *J. Geophys. Res.* **112**, B12309 (2007).
12. Newmark, R. L., Kasameyer, P. W. & Younker, L. W. Shallow drilling in the Salton-Sea Region—the thermal anomaly. *J. Geophys. Res.* **93**, 13005–13023 (1988).
13. Schmitt, A. K. & Vazquez, J. A. Alteration and remelting of nascent oceanic crust during continental rupture: Evidence from zircon geochemistry of rhyolites and xenoliths from the Salton Trough, California. *Earth Planet. Sci. Lett.* **252**, 260–274 (2006).
14. Waters, M. R. Late holocene lacustrine chronology and archaeology of ancient Lake Cahuilla, California. *Quat. Res.* **19**, 373–387 (1983).
15. Philibosian, B. *Paleoseismology of the San Andreas Fault at Coachella, California*. Master's thesis, Univ. Oregon (2007).
16. Kirby, S. M. *et al.* Pleistocene brawley and ocotillo formations: Evidence for initial strike-slip deformation along the San Felipe and San Jacinto fault zones, southern California. *J. Geol.* **115**, 42–62 (2007).
17. Hudnut, K. W., Seeber, L. & Pacheco, J. Cross-fault triggering in the November 1987 Superstition Hills earthquake sequence, Southern California. *Geophys. Res. Lett.* **16**, 199–202 (1989).
18. Burgmann, R. Transpression along the Southern San-Andreas Fault, Durmid Hill, California. *Tectonics* **10**, 1152–1163 (1991).
19. Larsen, S. & Reilinger, R. Age constraints for the present fault configuration in the Imperial Valley, California—evidence for Northwestward propagation of the Gulf of California Rift System. *J. Geophys. Res.* **96**, 10339–10346 (1991).
20. Johnson, C. E. & Hadley, D. M. Tectonic implications of the Brawley Earthquake Swarm, Imperial Valley, California, January 1975. *Bull. Seismol. Soc. Am.* **66**, 1133–1144 (1976).
21. Behr, W. *et al. SCEC Annual Meeting, Proceedings and Abstracts* Vol. 17, 87 (2007).
22. Meade, B. J. & Hager, B. H. Block models of crustal motion in southern California constrained by GPS measurements. *J. Geophys. Res.* **110**, B04402 (2005).
23. Hudnut, K. W., Seeber, L. & Rockwell, T. Slip on the Elmore Ranch Fault during the past 330 years and its relation to slip on the Superstition Hills Fault. *Bull. Seismol. Soc. Am.* **79**, 330–341 (1989).
24. Lohman, R. B. & McGuire, J. J. Earthquake swarms driven by aseismic creep in the Salton Trough, California. *J. Geophys. Res.* **112**, B04405 (2007).
25. Aydin, A. & Nur, A. Evolution of pull apart basins and their scale independence. *Tectonics* **1**, 91–105 (1982).
26. Steely, A. N., Janecke, S. U., Dorsey, R. J. & Axen, G. J. Early Pleistocene initiation of the San Felipe fault zone, SW Salton Trough, during reorganization of the San Andreas fault system. *Geol. Soc. Am. Bull.* **121**, 663–687 (2009).
27. Lutz, A. T., Dorsey, R. J., Housen, B. A. & Janecke, S. U. Stratigraphic record of Pleistocene faulting and basin evolution in the Borrego Badlands, San Jacinto fault zone, Southern California. *Geol. Soc. Am. Bull.* **118**, 1377–1397 (2006).
28. URS. Preliminary in-sea geotechnical investigation, Salton Sea Restoration Project Report (Riverside and Imperial Counties, 2004).
29. Meltzner, A. J., Rockwell, T. K. & Owen, L. A. Recent and long-term behavior of the Brawley Fault Zone, Imperial Valley, California: An escalation in slip rate? *Bull. Seismol. Soc. Am.* **96**, 2304–2328 (2006).
30. Kreemer, C., Holt, W. E. & Haines, A. J. An integrated global model of present-day plate motions and plate boundary deformation. *Geophys. J. Int.* **154**, 8–34 (2003).

Acknowledgements

Funding for this work was provided by the California Department of Water Resources, California Department of Fish and Game, UCSD Academic Senate, Scripps Institution of Oceanography, National Science Foundation (grants OCE-0112058 and EAR-0545250) and Southern California Earthquake Center (grant 2008-08127). We would like to thank B. Philibosian, D. Sandwell and D. Kilb for discussions, and V. Langenheim for a review.

Author contributions

D.S.B. planned field surveys, collected, analysed and interpreted the data and wrote the manuscript. N.W.D. and G.M.K. planned field surveys, collected and interpreted the data and provided extensive feedback on the manuscript. A.J.H., J.M.B. and R.L.B. collected data and provided feedback on the manuscript.

Additional information

Supplementary information accompanies this paper on www.nature.com/naturegeoscience. Reprints and permissions information is available online at http://npg.nature.com/reprintsandpermissions. Correspondence and requests for materials should be addressed to D.S.B.